Clim Dyn (2017) 48:2949–2965
DOI 10.1007/s00382-016-3243-z

The influence of boreal spring Arctic Oscillation on the subsequent winter ENSO in CMIP5 models

Shangfeng Chen[1] · Wen Chen[1] · Bin Yu[2]

Received: 28 December 2015 / Accepted: 17 June 2016 / Published online: 23 June 2016

Abstract This study examines the influence of boreal spring Arctic Oscillation (AO) on the subsequent winter El Niño-Southern Oscillation (ENSO) using 15 climate model outputs from the Coupled Model Intercomparison Project Phase 5 (CMIP5). Results show that, out of the 15 CMIP5 models, CCSM4 and CNRM-CM5 can well reproduce the significant AO–ENSO connection. These two models capture the observed spring AO related anomalous cyclone (anticyclone) over the subtropical western-central North Pacific, and westerly (easterly) winds over the tropical western-central Pacific. In contrast, the spring AO-related anomalous circulation over the subtropical North Pacific is insignificant in the other 13 models, and the simulations in these models cannot capture the significant influence of the spring AO on ENSO. Further analyses indicate that the performance of the CMIP5 simulations in reproducing the AO–ENSO connection is related to the ability in simulating the spring North Pacific synoptic eddy intensity and the spring AO's Pacific component. Strong synoptic-scale eddy intensity results in a strong synoptic eddy feedback on the mean flow, leading to strong cyclonic circulation anomalies over the subtropical North Pacific, which contributes to a significant AO–ENSO connection. In addition, a strong spring AO's Pacific component and associated easterly wind anomalies to its south may provide more favorable conditions for the development of spring AO-related cyclonic circulation anomalies over the subtropical North Pacific.

✉ Wen Chen
cw@post.iap.ac.cn

[1] Center for Monsoon System Research, Institute of Atmospheric Physics, Chinese Academy of Sciences, Beijing 100190, China

[2] Climate Research Division, Environment and Climate Change Canada, Toronto, ON, Canada

Keywords AO · ENSO · CMIP5 · Synoptic-scale eddy

1 Introduction

The Arctic Oscillation (AO) is the leading mode of atmospheric circulation variability over the northern extratropics on the interannual timescale (Thompson and Wallace 1998). Variability of AO can exert pronounced influences on weather and climate anomalies over many parts of the globe (e.g., Thompson and Wallace 1998, 2000; Gong et al. 2001, 2002, 2011; Wu and Wang 2002; Gong and Ho 2003; Chen et al. 2005, 2013a; Jeong and Ho 2005; Chen and Li 2007; Huang et al. 2007; Park et al. 2011; Cheung et al. 2012; Choi et al. 2012; Kim and Ahn 2012; Woo et al. 2012). For example, significant positive (negative) surface temperature anomalies can be observed over most parts of Eurasia when the boreal wintertime AO is in its positive (negative) phase (e.g., Thompson and Wallace 1998; Gong et al. 2001; Chen and Zhou 2012). Occurrence frequency of the wintertime cold surge over East Asia is below (above) normal when AO is in its positive (negative) phase (e.g., Jeong and Ho 2005). Studies also found that the variability of East Asian summer monsoon and tropical cyclonic activity can be significantly influenced by the spring AO (e.g., Gong and Ho 2003; Gong et al. 2011; Choi et al. 2012).

In the tropics, El Niño-Southern Oscillation (ENSO) is the strongest air–sea interaction system, which can exert substantial influences on the global climate and weather variability (e.g., Alexander 1992; Lau and Nath 1996; Zhang et al. 1997; Wang et al. 2000; Alexander et al. 2002; Wu et al. 2003, 2010; Huang et al. 2004; Yu and Zwiers 2007; Feng et al. 2011; Yeh et al. 2011; Zhou et al. 2013; Xue et al. 2015). Previous studies indicated that atmospheric circulation changes and associated sea surface temperature (SST) anomalies over extratropics are important in maintaining the ENSO variability (e.g., Vimont et al. 2001, 2003; Feng et al. 2014; Oshika et al. 2015; Nakamura et al. 2015; Ding et al. 2015; Chen et al. 2015a). For example, Vimont et al. (2003) showed that the boreal winter North Pacific Oscillation (NPO) can impact the outbreak of ENSO in the subsequent winter via the so-called "seasonal footprinting mechanism". NPO is defined as the second dominant mode of atmospheric variability over extratropics of the North Pacific (Rogers 1981; Linkin and Nigam 2008). Feng et al. (2014) reported that SST anomalies off Bajia California can be served as a precursor of an ENSO event. Using observational and reanalysis data, Oshika et al. (2015) reported that North Atlantic Oscillation (NAO) in the boreal winter has a significant linkage with the following winter ENSO variability. They demonstrated that the wintertime NAO influences the following winter ENSO via modulating the Eurasian snow cover and associated Asian cold air outbreak. In addition, the observed NAO–ENSO connection can also be captured by coupled climate models (Nakamura et al. 2015).

Recent studies indicated that the boreal spring AO could influence the following winter ENSO outbreak (e.g., Nakamura et al. 2006, 2007; Chen et al. 2013b, 2014, 2016). Nakamura et al. (2006, 2007) suggested that the influence is through modulating the anomalous westerly wind over the tropical western-central Pacific. Chen et al. (2014) further examined the physical process of this AO–ENSO connection and found that the interaction between synoptic-scale eddies and the low frequency mean flow and its associated vorticity transportation over the North Pacific play key roles in the formation of the spring AO-related cyclonic circulation anomalies over the subtropical Pacific. Significant atmospheric heating anomalies in association with the anomalous cyclone can also be observed over the subtropical North Pacific, which play an important role in maintaining the westerly wind anomalies over the tropical western-central Pacific via the Matsuno–Gill type atmospheric response (Matsuno 1966; Gill 1980). The anomalous westerly wind would trigger an eastward propagating and downwelling Kelvin wave that leads to positive SST anomalies over the tropical central-eastern Pacific (Barnett et al. 1989; Weisberg and Wang 1997; Wang and Weisberg 2000; Huang et al. 2001). Meanwhile, the positive SST anomalies over the tropical central-eastern Pacific are accompanied by atmospheric heating anomalies, which further maintain the westerly wind anomalies over the tropical Pacific. Through this positive air–sea feedback mechanism, an El Niño-like SST warming pattern is induced in the following winter.

Models are an important tool for investigating and understanding the climate variability. The Coupled Model Intercomparison Project Phase 5 (CMIP5) provides substantial simulation outputs for climate research (Taylor et al. 2012). Recent studies indicated that CMIP5 models have the ability to capture the atmospheric and oceanic circulation anomalies associated with ENSO (Deser et al. 2012; Bellenger et al. 2014; Gong et al. 2014) and AO (Zhu et al. 2013; Zuo et al. 2013). However, the connection between the boreal spring AO and the subsequent winter ENSO has not been explored in these models. The AO–ENSO relationship is an important aspect in evaluating the performance of climate models and improving the ENSO prediction skill. Hence, this study aims to address following three relevant questions: (1) Can the observed significant AO–ENSO connection be reproduced by the CMIP5 simulations? (2) Can these coupled models capture the observed physical process of the AO–ENSO connection? (3) What are the key factors responsible for model performances in simulating the AO–ENSO connection?

The rest of this paper is organized as follows: Sect. 2 describes the data and methods. Section 3 analyzes the ability of CMIP5 models in reproducing the spring AO–ENSO connection. Section 4 examines the physical process of the AO–ENSO relationship in these models that can simulate the connection. Section 5 discusses the factors responsible for model performances in reproducing the AO–ENSO connection. Section 6 provides a summary of this study.

2 Data and methods

2.1 Model data

We use the outputs from fifteen climate models in CMIP5 (available online at http://cmip-pcmdi.llnl.gov/cmip5/). At the time we performed this analysis, the daily mean geopotential height field, which is used to calculate the synoptic-scale eddy activity, was available from these fifteen climate models. Information (including Model ID, Institute and horizontal resolution) of these models is provided in Table 1. Since some models only provide one realization in daily and monthly mean variables, we adopt the first run of historical experiments from each model in this study. The historical experiments were performed with all forcing, including anthropogenic (e.g., greenhouse gases, anthropogenic aerosols, land use, and ozone) and natural (e.g., volcanic eruptions and solar radiation) sources (Taylor et al. 2012). The other analyzed variables include monthly mean sea level pressure (SLP), surface temperature, winds at 850 hPa, geopotential height at 500 and 200 hPa, and precipitation. Surface temperature over ocean areas represents SST. Chen et al. (2015b) have demonstrated that the influence of the spring AO on the subsequent winter ENSO experienced a significant interdecadal change around the early 1970s. Hence, the time period after 1975 is analyzed in this study. Note that results derived from the period after 1979 are similar.

Table 1 Information of the CMIP5 models used in this study

Model name	Modeling center	Resolution (lat, lon)
ACCESS1-0	Commonwealth Scientific and Industrial Research Organization and Bureau of Meteorology, Australia	144 × 192
bcc-csm1-1	Beijing Climate Center, China Meteorological Administration, China	64 × 128
CanESM2	Canadian Centre for Climate Modeling and Analysis, Victoria, BC, Canada	64 × 128
CCSM4	National Center for Atmospheric Research (NCAR) Boulder, CO, USA	192 × 288
CNRM-CM5	Centre National de Recherches Meteorologiques/Centre Europeen de Recherches et de Formation Avancee en Calcul Scientifique, France	128 × 256
FGOALS-s2	Institute of Atmospheric Physics, Chinese Academy of Sciences, China	108 × 128
GFDL-CM3	NOAA, Geophysical Fluid Dynamics Laboratory	90 × 144
GFDL-ESM2G	NOAA, Geophysical Fluid Dynamics Laboratory	90 × 144
GFDL-ESM2M	NOAA, Geophysical Fluid Dynamics Laboratory	90 × 144
HadGEM2-CC	Met Office Hadley Centre, United Kingdom	145 × 192
HadGEM2-ES	Met Office Hadley Centre, United Kingdom	145 × 192
IPSL-CM5A-LR	Institute Pierre Simon Laplace, Paris, France	96 × 96
IPSL-CM5B-LR	Institute Pierre Simon Laplace, Paris, France	96 × 96
MIROC-ESM	Japan Agency for Marine-Earth Science and Technology (JAMSTEC), Atmosphere and Ocean Research Institute (AORI), and National Institute for Environmental Studies (NIES), Japan	64 × 128
MIROC-ESM-CHEM	JAMSTEC, AORI, and NIES, Japan	64 × 128
MIROC5	AORI, NIES, JAMSTEC, Japan	128 × 256
MPI-ESM-LR	Max Planck Institute for Meteorology, Germany	96 × 192
MRI-CGCM3	Meteorological Research Institute, Japan	160 × 320
NorESM1-M	Norwegian Climate Centre, Norway	96 × 144

2.2 Observational data

The monthly mean SLP, geopotential height at 500 and 200 hPa, winds at 850 hPa, and precipitation are derived from the National Centers for Environmental Prediction-National Center for Atmospheric Research (NCEP-NCAR) reanalysis (Kalnay et al. 1996; ftp.cdc.noaa.gov/Datasets/). The monthly mean SST data are obtained from the National Oceanic and Atmospheric Administration (NOAA) Extended Reconstructed SST version 3b (ERSSTv3b) with a horizontal resolution of 2° × 2° (Smith et al. 2008; http://www.esrl.noaa.gov/psd/data/gridded). In this study, for convenience, the NCEP-NCAR reanalysis and ERSSv3b dataset are all called "observations". The period from 1975 to 2004 is used to compare against the CMIP5 data.

2.3 Methods

Following previous studies (e.g., Nakamura et al. 2006, 2007; Chen et al. 2014), spring is the average of March and April. The spring AO index is defined as the principle component time series corresponding to the first empirical orthogonal function (EOF) mode of spring area weighted SLP anomalies north of 20°N (Thompson and Wallace 1998). The Niño-3.4 index, defined as the area-averaged SST anomalies over the region of 5°S–5°N and 170°–120°W, is used to represent the ENSO variability (e.g., Anderson 2007; Deser et al. 2012).

To facilitate the comparison, all variables from observations and CMIP5 models are interpolated into a standard 2.5° × 2.5° grid. In addition, since we focus on investigating the interannual relationship between spring AO and ENSO, monthly mean anomalies of all variables are subjected to a 7-year high pass Lanczos filter (Duchon 1979). To avoid potential impacts of the ENSO cycle on the spring AO–ENSO connection, variability of all monthly mean variables that linearly correlated with the spring [March–April-averaged, MA(0)] Niño-3.4 SST index has been removed by a linear regression.

3 AO–ENSO connections in the observation and CMIP5 models

In this section, performances of the CMIP5 models in simulating the connection between the spring AO and the subsequent winter ENSO are investigated. We will compare the spring AO-related SST, precipitation and atmospheric circulation anomalies during the following winter in these models against those obtained from the observation.

Figure 1 displays the SST anomalies in the following winter [November–February-averaged, ND(0)JF(+1)] regressed upon the normalized spring AO index from 1975 to 2004 in the observation and in the 15 CMIP5 models. The time notations "(0)" and "(+1)" refer to the year during and after the spring AO year, respectively. In observation (Fig. 1a), during positive spring AO phases, significant and positive SST anomalies are observed over the tropical central-eastern Pacific, together with pronounced negative SST anomalies over the tropical western Pacific extending northeastward and southeastward to subtropical Pacific. The anomalous pattern shown in Fig. 1a bears a close resemblance to that associated with an El Niño event and is in good agreement with the feature described in previous studies (e.g., Nakamura et al. 2006, 2007; Chen et al. 2014).

Among the CMIP5 models, CCSM4 and CNRM-CM5 can well reproduce the observed spring AO-related SST pattern at ND(0)JF(+1) over the tropical Pacific (Fig. 1a, e, f), although the magnitude of SST anomalies are stronger in CCSM4 than those in CNRM-CM5 and observation (Fig. 1a, e, f). By contrast, the other thirteen models (i.e., ACCESS1-0, bcc-csm1-1, CanESM2, FGOALS-s2, GFDL-CM3, GFDL-ESM2G, GFDL-ESM2M, HadGEM2-CC, IPSL-CM5A-LR, IPSL-CM5B-LR, MIROC-ESM, MPI-ESM-LR, and NorESM1-M) cannot reproduce the spring AO-related SST anomalies during the subsequent winter (Fig. 1b–d, g–p). In these models, SST anomalies are weak and generally insignificant over the tropical Pacific.

Corresponding to above SST anomalies, similar model performances are identified in simulating the spring AO-related precipitation anomalies in the subsequent winter (Fig. 2). In response to the El Niño-like SST warming anomalies (Fig. 1a), the observation shows pronounced positive precipitation anomalies over the tropical central-eastern pacific and marked negative anomalies over the tropical western Pacific extending northeastward and southeastward to subtropical Pacific (Fig. 2a). CCSM4 and CNRM-CM5 are able to capture the observed ND(0) JF(+1) precipitation anomalies (Fig. 2e, f), with larger precipitation anomalies seen in CCSM4 than those in

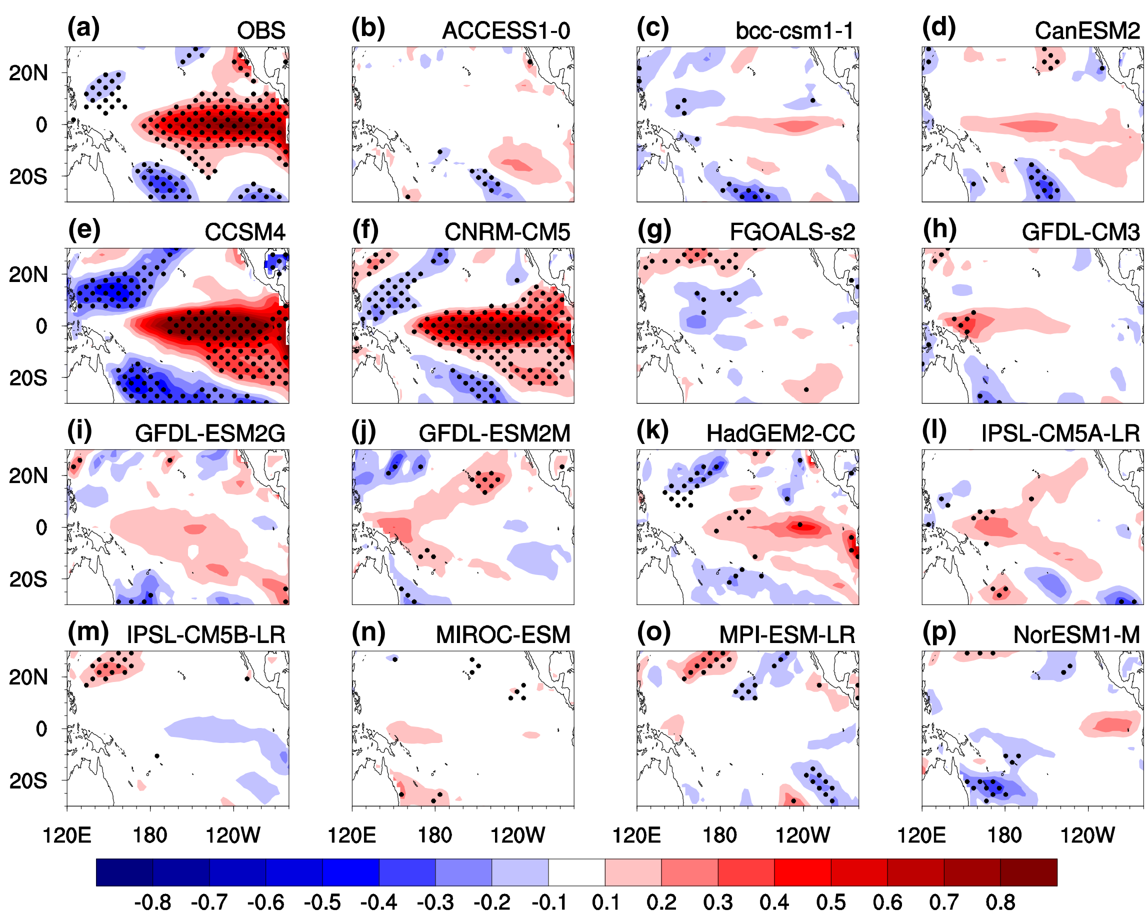

Fig. 1 Anomalies of SST in the following winter [November–February-averaged, ND(0)JF(+1)] obtained by regression upon the normalized spring [March–April-averaged, MA(0)] AO index during 1975–2004 in **a** observation and **b**–**p** 15 models runs from CMIP5 historical experiment. The model ID is shown at the *top right corner* of each figure. Anomalies significantly different from zero at the 5 % level in **a**–**p** are stippled. The SST unit is °C

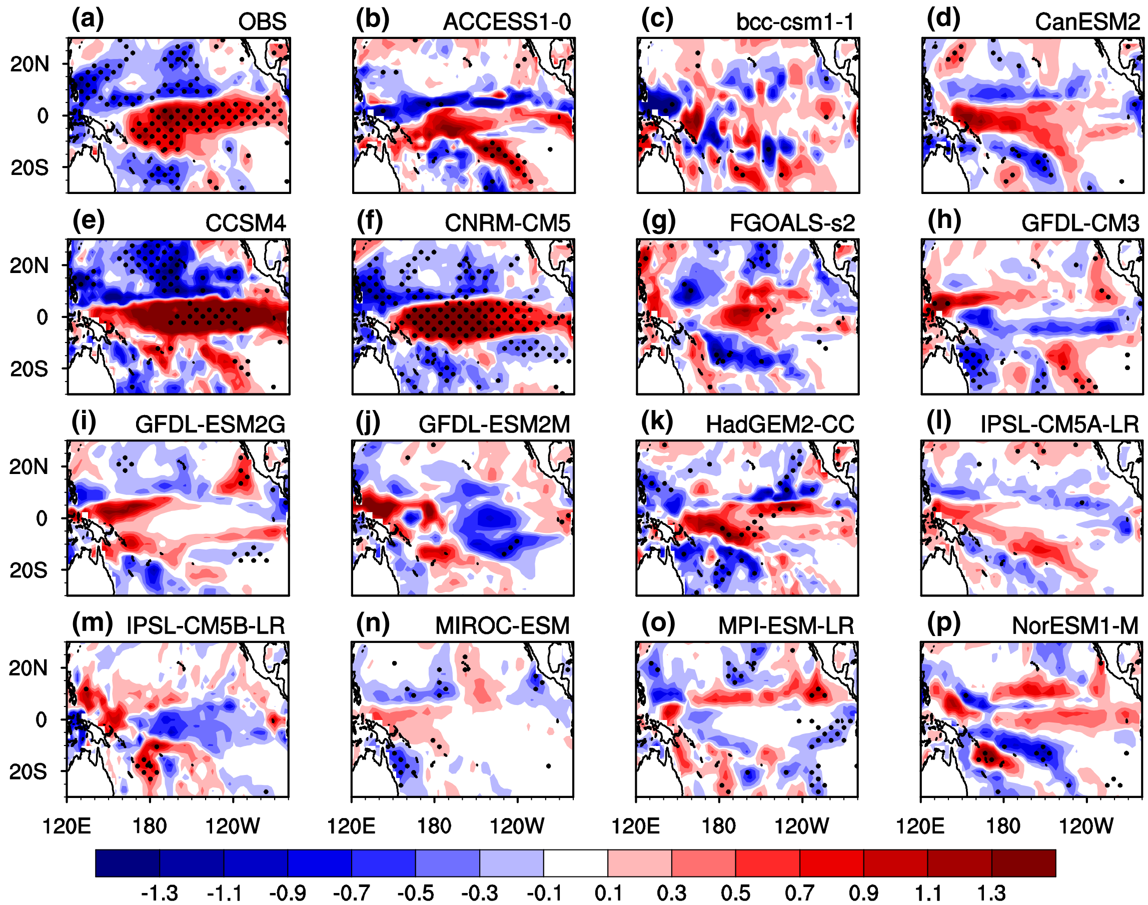

Fig. 2 The same as Fig. 1, except for precipitation anomalies at ND(0)JF(+1). The precipitation unit is mm day^{-1}

observation and CNRM-CM5 (Fig. 2a, e, f). In contrast, the precipitation anomalies at ND(0)JF(+1) are less well organized in the other thirteen models (Fig. 2b–d, g–p). Hence, out of the fifteen CMIP5 models analyzed in this study, CCSM4 and CNRM-CM5 are the only models that can simulate the observed AO–ENSO connection.

The correlation coefficient between the spring AO index and the subsequent winter Niño-3.4 index is further used to quantify the AO–ENSO relationship. Figure 3 displays the correlations over 1975–2004 in observation and 15 climate models. The correlation coefficients between the spring AO index and ND(0)JF(+1) Niño-3.4 index are 0.584, 0.359 and 0.364 in observation, CCSM4 and CNRM-CM5, respectively, all significant over the 5 % level. By contrast, the correlation coefficients are lower than 0.26 and insignificant at the 5 % level in other 13 models (Fig. 3). For convenience, these 13 models are classified as a "low correlation (LC)" model group in the following analysis. It is interesting to note that correlation coefficients between the spring AO and ND(0)JF(+1) Niño-3.4 index are negative (although insignificant at the 5 % level) in IPSL-CM5B-LR and MPI-ESM-LR, which are opposite to the observed value.

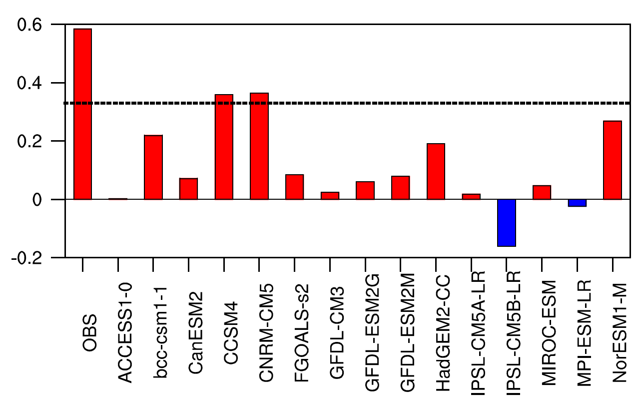

Fig. 3 Correlation coefficient between spring [MA(0)] AO index and subsequent winter [ND(0)JF(+1)] Niño-3.4 index during 1975–2004 in observation and 15 CMIP5 models. The model ID is shown at the *bottom*. *Horizontal dashed line* indicates the correlation exceeding the 5 % significance level

Figure 4 displays 850 hPa wind anomalies at ND(0)JF(+1) regressed upon the correspondingly normalized spring AO index in the observation, CCSM4,

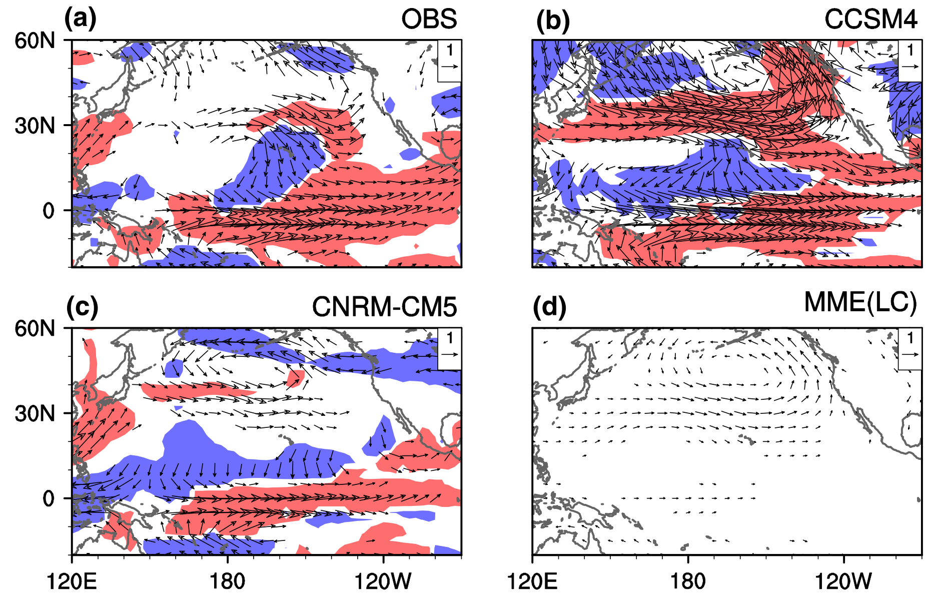

Fig. 4 Anomalies of ND(0) JF(+1) winds at 850 hPa obtained by regression upon the normalized spring AO index during 1975–2004 in **a** observation, **b** CCSM4, **c** CNRM-CM5, and **d** multimodel ensemble mean of 13 low correlation models [MME(LC)]. The *shading* in **a**–**d** denotes regions where either component of the wind anomalies is significantly different from zero at the 5 % level. The wind vector scale is shown in the *top right* with unit m s^{-1}

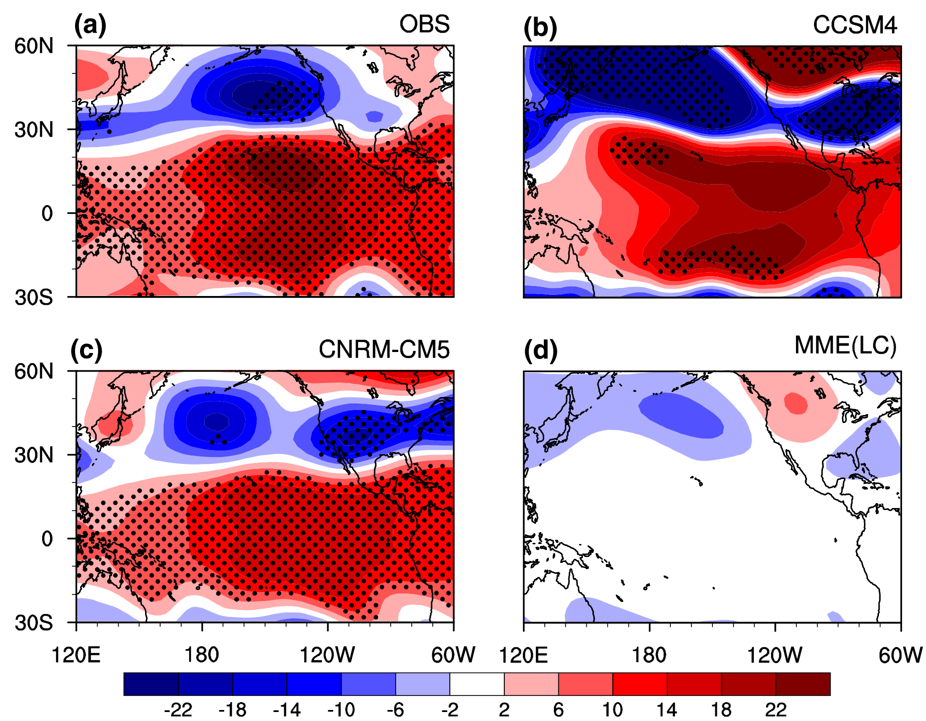

Fig. 5 The same as Fig. 4, except for ND(0)JF(+1) geopotential height anomalies (unit: m) at 200 hPa. Anomalies significantly different from zero at the 5 % level are stippled

CNRM-CM5, and multi-model ensemble mean of the LC model group, respectively. Figure 5 presents the associated 200 hPa geopotential height anomalies. In observation, significant westerly wind anomalies at 850 hPa are seen over the tropical central-eastern Pacific and easterly wind anomalies are observed over the tropical western Pacific (Fig. 4a). Meanwhile, a significant cyclonic circulation anomaly appears over midlatitudes of the North Pacific, indicating an intensified Aleutian Low. In addition, a pronounced anticyclonic circulation anomaly is found over the tropical western North Pacific. It has been demonstrated that the anomalous anticyclonic circulation over the tropical western North Pacific plays a key role in relaying the influence of El Niño on the East Asian climate anomalies (e.g., Wang et al. 2000). At 200 hPa, a Pacific-North America (PNA; Wallace and Gutzler 1981) teleconnection pattern can be observed over the Northern Hemisphere and the tropical Pacific is dominated by significant positive geopotential height anomalies in response to El Niño-like SST anomalies over the tropical central-eastern

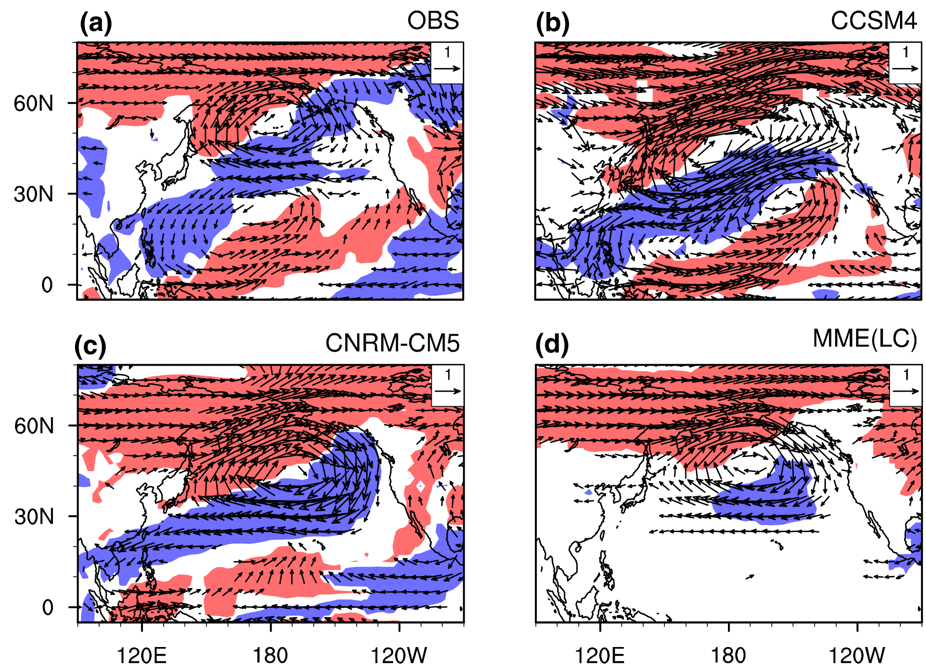

Fig. 6 Anomalies of MA(0) winds at 850 hPa obtained by regression upon the normalized spring AO index during 1975–2004 in **a** observation, **b** CCSM4, **c** CNRM-CM5, and **d** multimodel ensemble mean of 13 low correlation models [MME(LC)]. The *shading* in **a**–**d** denotes regions where either component of the wind anomalies is significantly different from zero at the 5 % level. The wind vector scale is shown in the *top right corner* of each figure with unit m s^{-1}

Pacific (Fig. 5a). Overall, the anomalous patterns of the spring AO-related 850 hPa winds and 200 hPa geopotential height bear a close resemblance to those associated with an El Niño event, consistent with the results obtained in the previous study using the NCEP data from 1958 to 2010 (Chen et al. 2014). From Figs. 1, 4 and 5, anomalies of SST and atmospheric circulation over North Pacific at ND(0)JF(+1) in association with preceding spring AO are stronger in CCSM4 than in observation. However, the correlation between the spring AO and ND(0)JF(+1) Niño-3.4 index is larger in observation (Fig. 3). This may be attributed to the fact that standard deviation (amplitude) of the tropical SST and North Pacific atmospheric circulation are much larger in CCSM4 than those in observation (figures not shown), which can lead to a lower correlation relative to a regression in CCSM4.

CCSM4 and CNRM-CM5 are able to reproduce the main circulation anomalies described above, with differences mainly in magnitude (Figs. 4b, c, 5b, c). Deser et al. (2012) have reported that the seasonal atmospheric teleconnections associated with ENSO are generally well simulated by CCSM4. The magnitude of atmospheric circulation anomalies associated with the spring AO is larger in CCSM4 than those in CNRM-CM5 and observation (Figs. 4a–c, 5a–c), accompanied by the stronger SST and precipitation anomalies in CCSM4 (Fig. 1e, e). By contrast, the spring AO-related atmospheric circulation anomalies in the following winter are weak except those over the North Pacific in the multimodel ensemble mean of the LC models (Figs. 4d, 5d).

4 Physical processes for the influence of AO on ENSO in CMIP5 models

Here, the physical process of the AO–ENSO connection is examined by analyzing the spring AO-related atmospheric circulation, precipitation and SST anomalies in the simultaneous spring, and the evolution of these anomalies from spring to winter.

4.1 Atmospheric circulation, precipitation and SST anomalies in spring

Figure 6 displays the 850 hPa wind anomalies in spring regressed upon the normalized spring AO index in observation, CCSM4, CNRM-CM5, and multimodel ensemble mean of the LC models, respectively. In the observation, a significant atmospheric dipole can be observed at 850 hPa, with a pronounced anticyclonic circulation anomaly over midlatitudes of the North Pacific, and a notable cyclonic circulation anomaly over the subtropical western-central Pacific (Fig. 6a). This is consistent with the results obtained in previous studies based on different datasets (e.g., Nakamura et al. 2007; Gong et al. 2011; Chen et al. 2014). CCSM4 and CNRM-CM5 are able to reproduce the anomalous atmospheric pattern over the Pacific Ocean (Fig. 6b, c). In particular, significant westerly wind anomalies can be observed over the tropical western-central Pacific in CCSM4 and CNRM-CM5 (Fig. 6b, c), which are important for the ENSO evolution in the subsequent winter. Note that the dipole atmospheric circulation anomaly pattern over

Fig. 7 Anomalies of MA(0) precipitation (unit: mm day^{-1}) obtained by regression on the normalized spring AO index during 1975–2004 in **a** observation, **b** CCSM4, **c** CNRM-CM5, and **d** multimodel ensemble mean of 13 low correlation models [MME(LC)]. Anomalies significantly different from zero at the 5 % level are stippled

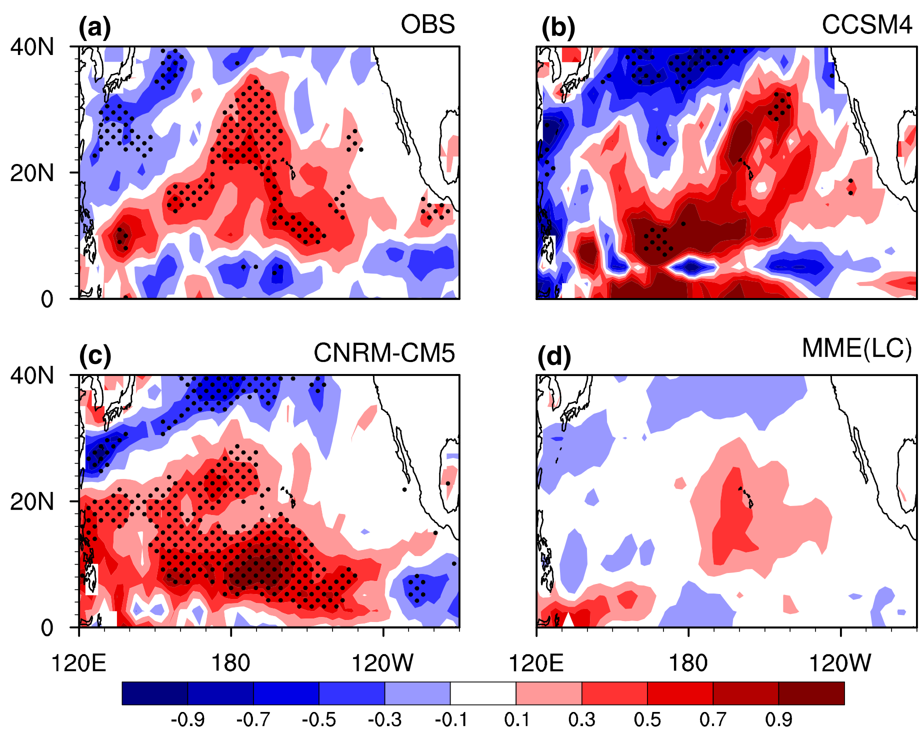

the North Pacific captured by the observation, CCSM4 and CNRM-CM5 bears some resemblances to that associated with NPO during preceding winter (Fig. 6a–c) (e.g., Vimont et al. 2001, 2003). Vimont et al. (2003) have demonstrated that boreal winter NPO can exert an influence on the subsequent winter ENSO outbreak via the seasonal footprinting mechanism, which involves air–sea interactions over the North Pacific. This implies that variability of NPO during preceding winter may also play a role in the formation of the dipole atmospheric circulation anomaly during the following spring over the North Pacific (Fig. 6a–c). In comparison, only the anticyclonic circulation anomaly over the North Pacific is captured by the LC models (Fig. 6d). The anomalous cyclonic circulation and its associated westerly wind anomalies are extremely weak and disappear over the tropical western-central Pacific in the LC models (Fig. 6d). The anomalous circulation in the LC models is not in favor for the ENSO evolution. The reason that the spring AO-related cyclonic circulation anomalies over the subtropical North Pacific are stronger in CCSM4 and CNRM-CM5 than those in the LC models will be discussed in Sect. 5.

Maintenance of the anomalous cyclonic circulation over the subtropical North Pacific and the associated westerly wind anomalies over the tropical western North Pacific from spring to summer are related to the atmospheric heating anomalies over the subtropical North Pacific (Chen et al. 2014). There is positive feedback between atmospheric circulation and atmospheric heating anomalies there. The atmospheric heating anomalies may induce cyclonic circulation anomalies over the subtropical North Pacific via a Gill type atmospheric response. The anomalous cyclonic circulation could subsequently lead to local SST warming via reducing the climatological easterly winds and in turn enhance the atmospheric heating (Chen et al. 2014). It has been demonstrated that precipitation anomalies can be used to represent the atmospheric heating anomalies to a large extent (Yu and Zwiers 2007; Chen et al. 2014). Figure 7 displays the corresponding precipitation anomalies. In observation, significant and positive precipitation anomalies are seen over the subtropical western-central North Pacific (Fig. 7a), consistent with Chen et al. (2014). The anomalous precipitation plays an important role in maintaining the spring AO-related cyclonic circulation anomalies through the Matsuno–Gill type atmospheric response. The CCSM4 and CNRM-CM5 can well reproduce the spring AO-related positive precipitation anomalies over the subtropical western-central North Pacific (Fig. 7b, c). By contrast, positive precipitation anomalies are not significant and weaker in the LC models than those in CCSM4, CNRM-CM5 (Fig. 7b–d).

Figure 8 further shows the spring SST anomalies regressed upon the normalized spring AO index in observation, CCSM4, CNRM-CM5, and ensemble mean of the LC models, respectively. In observation, a tripole SST anomaly pattern can be seen over the Pacific Ocean, with positive anomalies over the tropical central Pacific extending northeastward to the west coast of North America and over the midlatitudes of North Pacific, and negative anomalies over

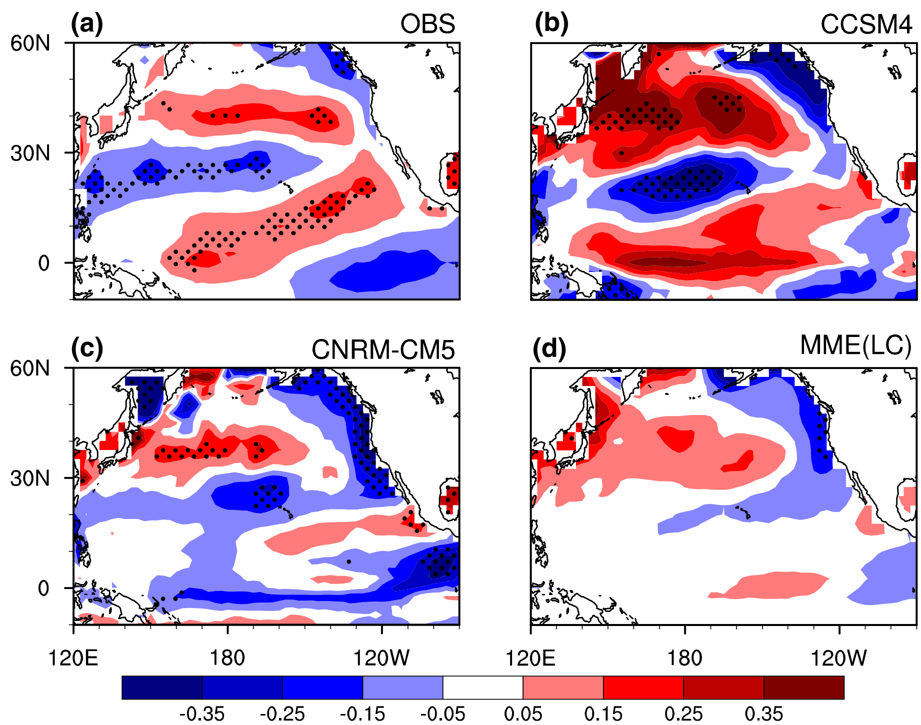

Fig. 8 The same as Fig. 7, except for MA(0) SST (unit: °C) anomalies. Anomalies significantly different from zero at the 5 % level are stippled

the subtropical western-central North Pacific (Fig. 8a). Note that this tripole SST anomaly pattern related to the spring AO over the North Pacific is similar to that associated with the Pacific Meridional mode (Chiang and Vimont 2004). The Pacific Meridional mode has been suggested as a potential bridge in linking the extratropical atmospheric variability to the tropical climate (Chiang and Vimont 2004). This implies that the Pacific Meridional mode may play a role in linking the spring AO to the following winter ENSO events, which remains to be explored. In addition, Lin et al. (2015) found that the CMIP5 coupled models can reasonably capture the spatial pattern of the Pacific Meridional mode. The CCSM4 and CNRM-CM5 can reasonably reproduce the tripole SST anomaly pattern, although the anomalies are relatively weak in CNRM-CM5, and strong in CCSM4 (Fig. 8b, c). In contrast, SST anomalies in the tropical and subtropical North Pacific are extremely weak in the LC model ensemble mean (Fig. 8a). This may be attributed to the fact that the simultaneous spring cyclonic circulation anomalies over the subtropical western-central North Pacific are very weak in the LC models (Fig. 6d). Previous studies have found that the formation of spring SST anomalies over the North Pacific are mainly resulted from the surface heat flux changes associated with the anomalous atmospheric circulation (Gong et al. 2011; Hu et al. 2013; Chen et al. 2014). For example, in observation, westerly wind anomalies over the tropical central Pacific reduce the climatological easterly winds, leading to positive SST anomalies there through a reduction of evaporation (Figs. 6a, 8a). The negative SST anomalies in the subtropical western North Pacific may be related to enhanced evaporation associated with northeasterly winds there (Figs. 6a, 8a) (Chen et al. 2014).

4.2 Evolution of atmospheric circulation, precipitation and SST anomalies

In the following, evolution of the spring AO-related atmospheric circulation, SST and precipitation anomalies over the tropical Pacific is further investigated. Figure 9 displays the anomalies of the equatorial (5°S–5°N-averaged) zonal winds at 850 hPa, SST, and precipitation from the simultaneous March to the following December regressed upon the normalized spring AO index in the observation, CCSM4 and CNRM-CM5, respectively. In observation, significant westerly wind anomalies are seen over the tropical western Pacific in the simultaneous spring (Fig. 9a). The westerly wind anomalies over the tropical western Pacific persist from spring to the following summer, which may be attributed to the atmospheric heating anomalies over the subtropical North Pacific (Fig. 7a), and then propagate eastward to the tropical central-eastern Pacific in the following autumn (Fig. 9a). Associated with the westerly wind anomalies, pronounced positive SST anomalies are observed in the tropical western Pacific in spring and summer, and then propagate eastward into the tropical central-eastern Pacific in the subsequent autumn (Fig. 9b). Significant and positive precipitation anomalies can be observed over the tropical central-eastern Pacific in the autumn as a response to positive SST anomalies there. The tropical atmospheric

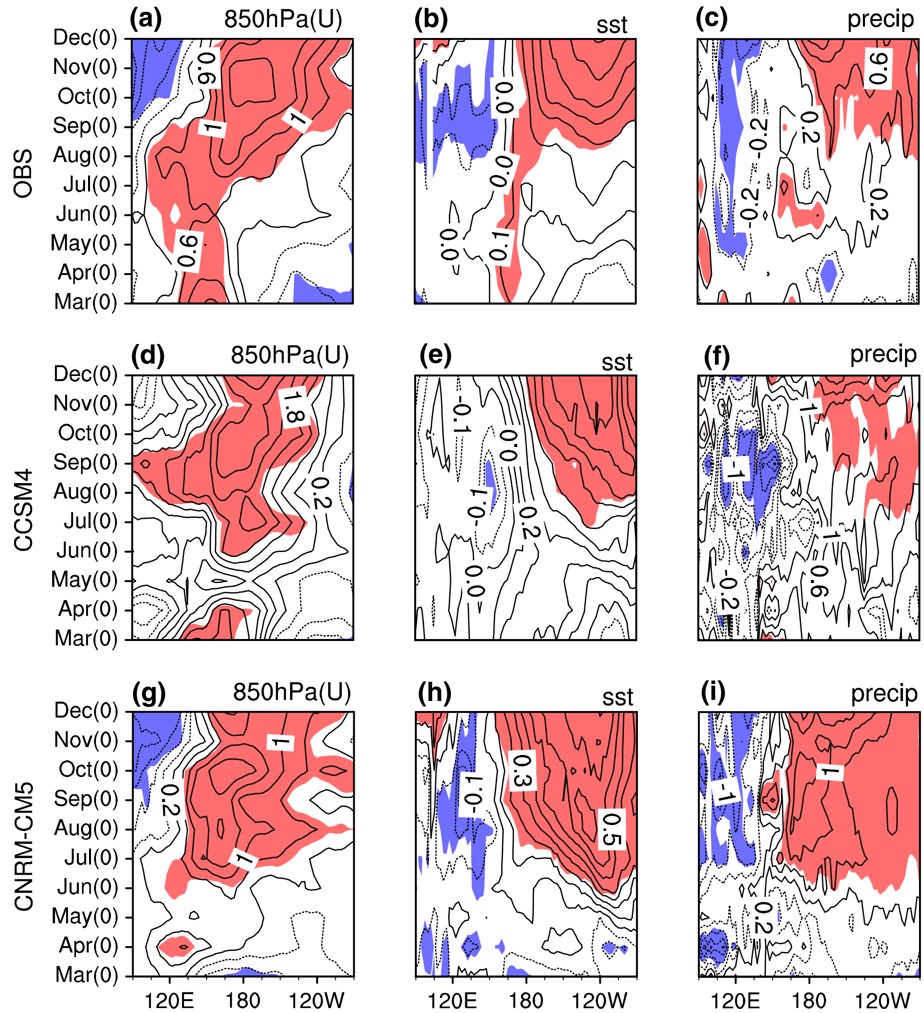

Fig. 9 Anomalies of the equatorial (5°S–5°N-averaged) **a** 850 hPa zonal winds, **b** SST, and **c** precipitation from simultaneous March to following December regressed upon the normalized spring AO index during 1975–2004 in observation. **d**–**f**, **g**–**i** as in **a**–**c**, but the data are derived from CCSM4 and CNRM-CM5, respectively. The *shading* in **a**–**i** indicates the anomalies that are significantly different from zero at the 5 % level. Contour intervals are 0.2 m s^{-1} in **a**, **d**, **g**, 0.1 °C in **b**, **e**, **h**, and 0.4 mm day^{-1} in **c**, **f**, **i**

circulation, tropical heating and SST anomalies can sustain and develop into the following winter via the positive Bjerknes-like air–sea feedback mechanism (Bjerknes 1969). The evolutions of 850 hPa zonal wind, SST and precipitation anomalies in CCSM4 and CNRM-CM5 bear close resemblance to those in the observation (Fig. 9), indicating that CCSM4 and CNRM-CM5 are able to reproduce the tropical air–sea interaction associated with the spring AO. In contrast, evolution of tropical atmospheric circulation, SST and precipitation is not obvious in the LC model ensemble (figures not shown).

5 Possible reasons for different model performances in simulating the spring AO–ENSO connection

Results in the previous section suggested that the performance of a CMIP5 climate model in simulating the AO–ENSO relationship mainly depends on whether the model can well capture the cyclonic circulation anomalies over the subtropical North Pacific. As demonstrated in previous studies (e.g., Gong et al. 2011; Chen et al. 2014), the development of the spring AO related cyclonic circulation and its associated negative geopotential height anomalies over the subtropical North Pacific are attributed to the interaction between synoptic-scale eddies and the low frequency mean flow and the accompanied vorticity transportation. The interaction between synoptic eddy and low frequency mean flow is an important internal source in forming and maintaining atmospheric circulation anomalies related to AO (e.g., Limpasuvan and Hartmann 1999, 2000; Lorenz and Hartmann 2003; Thompson et al. 2003). In positive AO phases, a significant anticyclonic circulation anomaly exists in the Aleutian region (Fig. 6a). Accompanied with this anomalous anticyclonic circulation, significant easterly wind anomalies are seen over midlatitudes of North Pacific, indicating a weakened westerly jet stream. Based on Lau (1988), weakening of the westerly jet stream is accompanied by weakened synoptic-scale eddy activity, as well as negative geopotential height tendency immediately to its south and positive geopotential height tendency to its north.

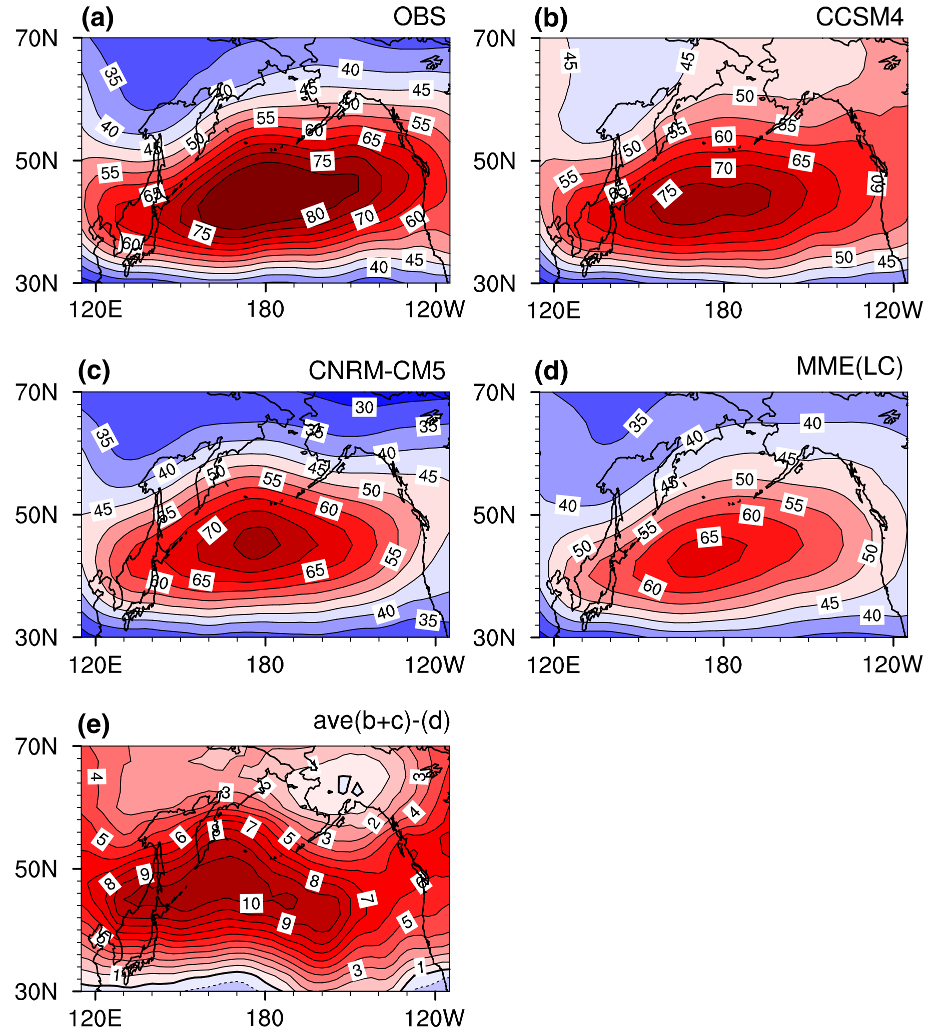

Fig. 10 Spring [MA(0)] storm track activity (m) averaged from 1975 to 2004 in **a** observation, **b** CCSM4, **c** CNRM-CM5, and **d** multimodel ensemble mean of 13 low correlation models. **e** Result of the average between (**b**) and (**c**) minus (**d**). Contour intervals are 5 m in **a**–**d**, and 1 m in **e**

Hence, the feedback of synoptic scale eddy to low frequency mean flow may explain the formation of the negative geopotential height and cyclonic circulation anomalies over the subtropical North Pacific.

The spring AO-related cyclonic circulation anomalies are stronger and a much greater portion of the Pacific exhibits significant anomalies in observations, CCSM4 and CNRM-CM5 than those in the LC models (Fig. 6). This implies that the intensity of the eddy–mean flow interaction is stronger in observation, CCSM4 and CNRM-CM5 than that in the LC models. Previous studies suggested that the eddy–mean flow interaction strength is related to several factors, including the intensity of the synoptic-scale eddy, the eddy spatial length scale and its life time (e.g., Jin et al. 2006a, b; Jin 2010). Among those factors, the intensity of synoptic eddy is a key component in determining the strength of synoptic eddy feedback to low frequency mean flow. Specifically, the strength of the synoptic eddy feedback is proportional to the synoptic-scale eddy intensity, given the same magnitude of low-frequency mean flow (e.g., Jin et al. 2006a, b; Jin 2010). Hence, it is reasonably hypothesized that the intensity of the synoptic scale eddy activity is stronger in observation, CCSM4, and CNRM-CM5 than that in the LC models.

Figure 10a–d display spring the synoptic eddy activity (m) at 250 hPa averaged from 1975 to 2004 in the observation, CCSM4, CNRM-CM5, and the LC models, respectively. Figure 10e shows the difference between high correlation models (average of CCSM4 and CNRM-CM5) and LC models. The synoptic-scale eddy activity is defined as the root mean square of the 2–8 day band pass filtered daily mean geopotential height at this level (e.g., Chang and Fu 2002; Lee et al. 2012; Chen et al. 2014). Note that results in other pressure levels (e.g., 850 and 500 hPa) are similar to those derived from 250 hPa (not shown). A center of action of synoptic scale eddy activity can be observed over the midlatitudes of North Pacific in the observation, CCSM4, CNRM-CM5 and LC models, consistent with previous studies (e.g., Lee et al. 2012; Chen et al. 2014). This implies that the CMIP5 models can well simulate the

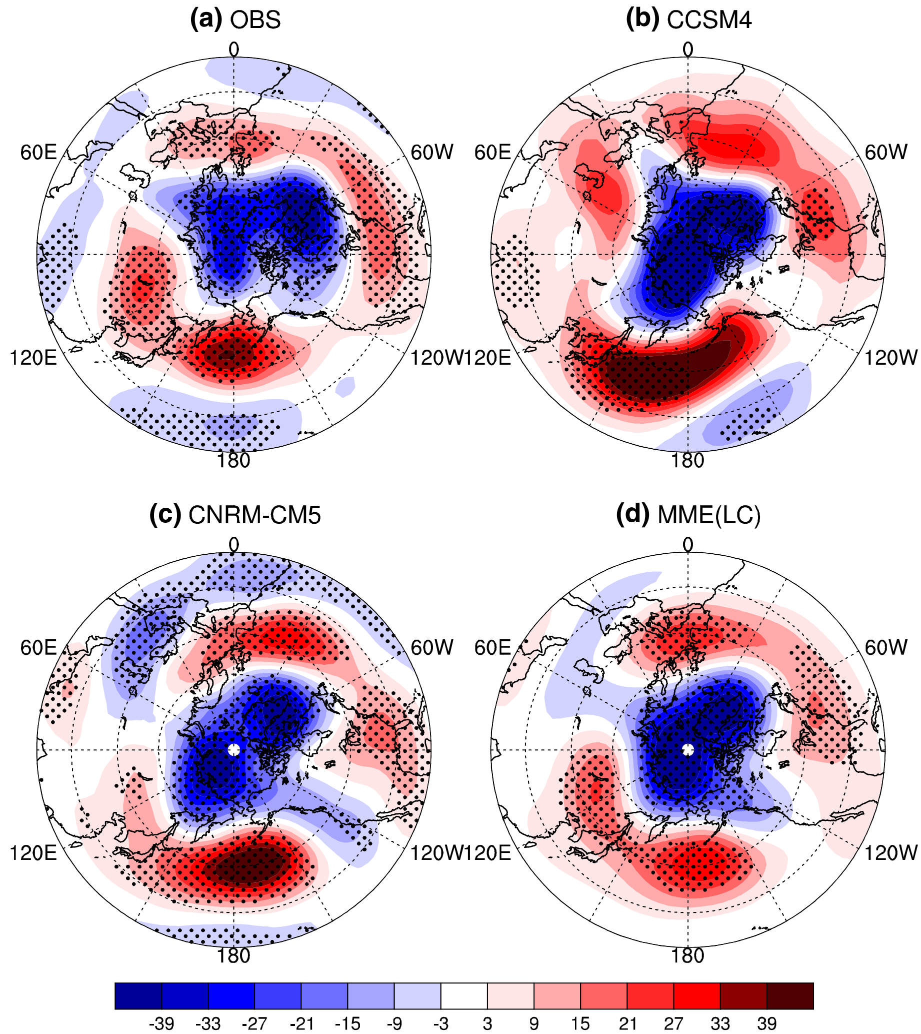

Fig. 11 Anomalies of geopotential height at 500 hPa (unit: m) in spring [MA(0)] obtained as regression upon the normalized spring AO index during 1975–2004 in **a** observation, **b** CCSM4, **c** CNRM-CM5, and **d** multimodel ensemble mean of 13 low correlation models [MME(LC)]. Anomalies significantly different from zero at the 5 % level are stippled

climatological spatial pattern of the synoptic-scale eddy activity over the North Pacific. However, the intensity of synoptic eddy over the midlatitudes of North Pacific is stronger in the observation, CCSM4 and CNRM-CM5 than that in the LC models by about 10 m (Fig. 10e). In particular, the maximum values of spring synoptic scale eddy exceed 80, 75, and 75 m in the observation, CCSM4, and CNRM-CM5, respectively. By contrast, the eddy magnitude is about 65 m in the LC model mean. Above results indicate that feedback strength of synoptic-scale eddy to low frequency mean flow is stronger in the observation, CCSM4, and CNRM-CM5 than that in the LC models. It should be noted that there are models with spring storm track activity close to observation over North Pacific, accompanied by weak AO–ENSO connection (such as ACCESS1-0 and FGOALS-s2, figures not shown). This indicates that the spring storm activity over the North Pacific cannot fully determine the connection between spring AO and subsequent ENSO in CMIP5 models. Chang et al. (2012) also evaluated the performance of CMIP5 models in simulating the synoptic-scale eddy activity (also called storm track). They found that the simulated storm track in most of the CMIP5 models are much weaker and shift equatorward compared to that in observation.

Previous studies also indicated that the intensity of the spring AO's Pacific component may influence the development of the cyclonic circulation anomalies over the subtropical North Pacific (e.g., Gao et al. 2013). Figure 11 displays the anomalies of geopotential height at 500 hPa in spring regressed upon the normalized spring AO index in the observation, CCSM4, CNRM-CM5, and LC models. Significant and negative geopotential anomalies are seen over the Arctic region and significant and positive geopotential height anomalies are observed over midlatitudes of North Pacific in the observation, CCSM4 and CNRM-CM5 (Fig. 11a–c). In particular, significantly negative geopotential height anomalies, which correspond to cyclonic circulation anomalies (Fig. 6a–c), can be seen over the subtropical North Pacific in the observation, CCSM4 and CNRM-CM5 (Fig. 11a–c). In contrast, the negative

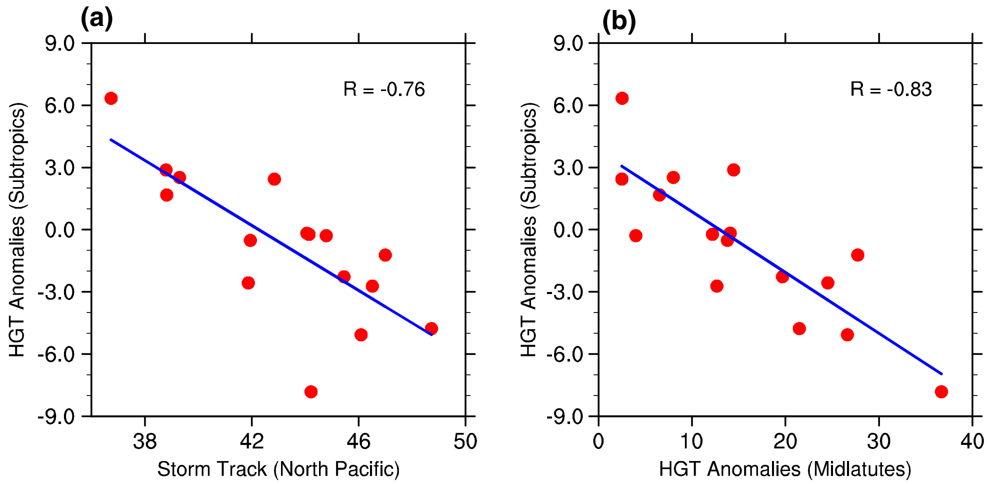

Fig. 12 *Scatter plots* of 500 hPa spring geopotential height anomalies averaged over the subtropical North Pacific (10°–30°N and 150°E–150°W) with spring **a** climatological storm track activity averaged over the North Pacific (40°–50°N and 120°E–110°W), and **b** 500 hPa geopotential height anomalies averaged over midlatitudes of North Pacific (45°–60°N and 120°E–150°W) in 15 CMIP5 models and observation. The best fitting lines are indicated by *blue solid lines*

geopotential height anomalies over the subtropical North Pacific cannot be detected in the LC model mean. In addition, intensities of the spring AO's Pacific component over the midlatitude of North Pacific are also stronger in the observation, CCSM4, and CNRM-CM5 than those in the LC models. Accordingly, the spring-AO related easterly wind anomalies over the midlatitudes of North Pacific are stronger in the observation, CCSM4 and CNRM-CM5 than that in the LC models (not shown). The weak spring AO-related easterly wind anomalies may impede the development of the cyclonic circulation anomalies over the subtropical North Pacific in the LC models.

Figure 12 presents further evidence to confirm the assertion that the model's performance in capturing negative geopotential height anomalies and associated cyclonic circulation anomalies over the subtropical North Pacific is closely related to the model's ability in reproducing the spring North Pacific synoptic eddy intensity and the spring AO's Pacific component. Figure 12a displays a scatter diagram between spring 500 hPa geopotential height anomalies over the subtropical North Pacific and the climatological spring 500 hPa storm track over North Pacific. Figure 12b shows a scatter plot between spring 500 hPa geopotential height anomalies over the subtropical North Pacific and over midlatitudes of North Pacific. Results indicate that the CMIP5 models that produce stronger negative geopotential height anomalies over the subtropical North Pacific tend to have stronger spring climatological North Pacific storm track intensity and stronger positive geopotential height anomalies over midlatitudes of North Pacific. The correlations between the two quantities shown in Fig. 12a, b are as high as −0.76 and −0.83, respectively, which are statistically significant at the 1 % level based on the Student's *t* test. The result supports our assertion that the performance of the CMIP5 models in reproducing the negative geopotential height anomalies and associated anomalous cyclonic circulation over the subtropical North Pacific are closely related to the model's performance in simulating the spring North Pacific synoptic eddy intensity and spring AO's Pacific component (Figs. 10, 11).

Finally, we examine whether the performance of a CMIP5 model in capturing the AO–ENSO connection is related to its ability in simulating the ENSO variability. To address this issue, we show the standard deviations of ND(0)JF(+1) SST anomalies during 1975–2004 in the observation, CCSM4, CNRM-CM5, and the LC models in Fig. 13. It is found that spatial pattern of the SST variability in the tropical Pacific in the LC models bear a close resemblance to those in the observation, CCSM4 and CNRM-CM5 (Fig. 13). Note that the magnitude of SST variability over the tropical Pacific, especially around the Niño-4 region (5°S–5°N and 160°E–150°W), is weaker in the LC models than that in the observation, CCSM4 and CNRM-CM5 (Fig. 13). To examine whether the AO–ENSO connection in CMIP5 models is related to the ENSO variability over the tropical Pacific, a scatter plot between the SST variability in the Niño-4 region and the AO–ENSO correlation is presented in Fig. 14. It can be seen that the models producing a stronger AO–ENSO connection do not necessary have a stronger SST variability in the tropical Pacific. The correlation coefficient between the two quantities is merely 0.07, which is insignificant at the 5 % level. This indicates that the ability of the CMIP5 models in reproducing the AO–ENSO connection may not be related to the

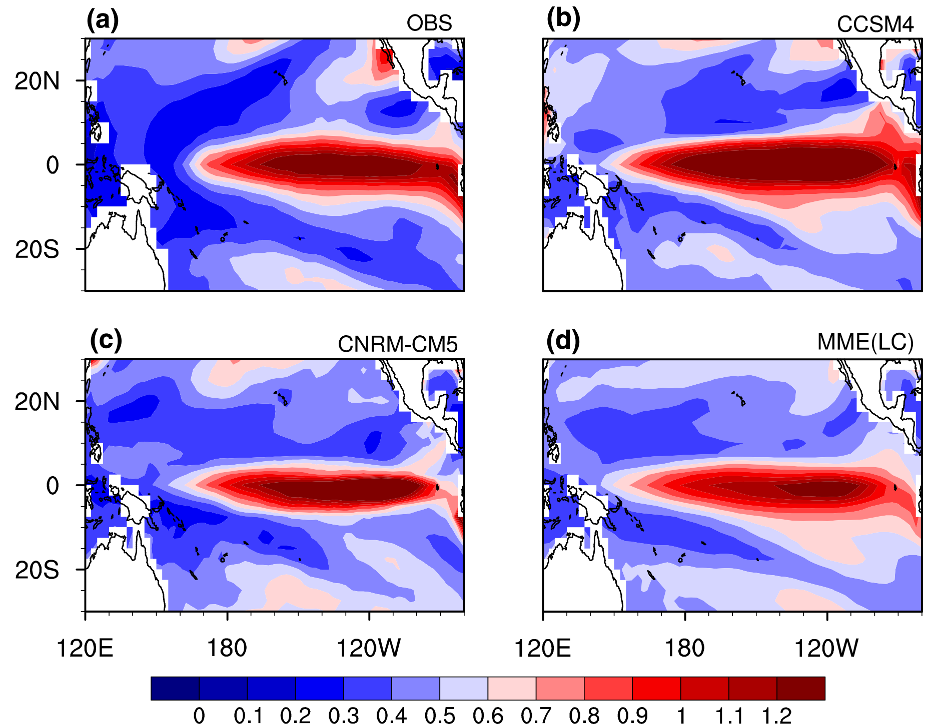

Fig. 13 Standard deviation of ND(0)JF(+1) SST (unit: °C) during 1975–2004 in **a** observation, **b** CCSM4, **c** CNRM-CM5, and **d** multimodel ensemble mean of 13 low correlation models

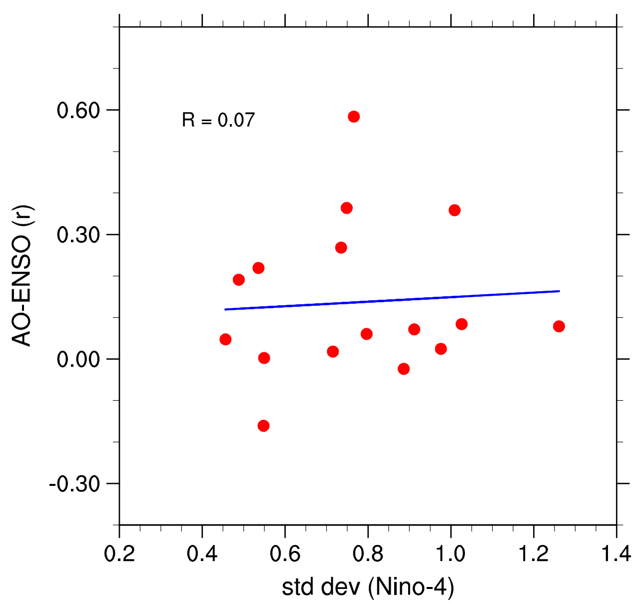

Fig. 14 *Scatter plot* between the AO–ENSO correlation and the standard deviation of SST in Niño-4 region (5°S–5°N and 160°E–150°W) in 15 CMIP5 models and observation. The best fitting line is indicated by the *blue solid line*

ability of a model in simulating the ENSO variability, and suggests that other mechanisms play important roles in the ENSO variability as well.

Results in this section suggest that the performance of the CMIP5 simulations in reproducing the AO–ENSO connection is mainly related to the performance of the models in simulating the spring synoptic-scale eddy activity in the North Pacific and the AO's Pacific component. A stronger synoptic eddy feedback to the low frequency mean flow is associated with stronger cyclonic circulation anomalies over the subtropical North Pacific and stronger AO's Pacific component in CCSM4 and CNRM-CM5 than those in the LC models.

6 Summary

Previous studies have suggested that the boreal spring AO can exert a pronounced influence on the subsequent winter ENSO (e.g., Nakamura et al. 2006, 2007; Chen et al. 2014). In this study, the AO–ENSO connection in fifteen CMIP5 coupled models is evaluated against the observational data (NCEP-NCAR reanalysis and ERSSTv3b). First, we calculate the spring AO-related SST, precipitation and atmospheric circulation anomalies in the following winter to examine the performance of these models in reproducing the observed AO–ENSO connection. The results indicate that CCSM4 and CNRM-CM5 are able to capture the significant influence of the spring AO on the subsequent winter ENSO, while the influence is not captured in the other 13 models.

The physical processes of the AO–ENSO connection in CCSM4 and CNRM-CM5 are further investigated. Results show that CCSM4 and CNRM-CM5 can well reproduce the observed spring AO-related anomalies of cyclonic circulation and atmospheric heating over the subtropical North Pacific, and westerly winds in the tropical western-central Pacific in the simultaneous spring. In addition, the evolution of tropical Pacific atmospheric circulation, SST, and atmospheric heating anomalies from spring to the following winter in CCSM4 and CNRM-CM5 also bear close resemblances to those in the observation. In contrast, the spring AO-related cyclonic circulation and associated atmospheric heating anomalies over the subtropical North Pacific are very weak and almost disappear in the LC models. Hence, the spring AO–ENSO connection cannot be reproduced in these LC models.

Finally, we examine the possible reasons that the thirteen LC models cannot capture the AO–ENSO relationship. Generally, in the LC models, the synoptic-scale eddy intensity and the spring AO's Pacific components are underestimated. The weaker synoptic-scale eddy intensity leads to a weaker synoptic eddy feedback to low frequency mean flow, and results in weaker cyclonic circulation anomalies over the subtropical North Pacific in the LC models than those in CCSM4 and CNRM-CM5. In addition, the weak spring AO's Pacific component and the associated weak easterly wind anomalies over the midlatitudes of North Pacific may also prevent the development of the cyclonic circulation anomalies over the subtropical North Pacific in the LC models.

Acknowledgments We thank the three anonymous reviewers for their valuable comments and suggestions, which led to significant improvement in the manuscript. We acknowledge the World Climate Research Programme's Working Group on Coupled Modeling, which is responsible for CMIP, and we thank the climate modeling groups (listed in Table 1 of this paper) for producing and making available their model output. For CMIP the U.S. Department of Energy's Program for Climate Model Diagnosis and Intercomparison provides coordinating support and led development of software infrastructure in partnership with the Global Organization for Earth System Science Portals. This study is supported by the Project Funded by China Postdoctoral Science Foundation (2015M581151) and the National Natural Science Foundation of China Grants (41230527, 41530425).

References

Alexander MA (1992) Midlatitude atmosphere–ocean interaction during El Niño. Part I: the North Pacific Ocean. J Clim 5(9):944–958

Alexander MA, Bladé I, Newman M, Lanzante JR, Lau N-C, Scott JD (2002) The atmospheric bridge: the influence of ENSO teleconnections on air–sea interaction over the global oceans. J Clim 15(16):2205–2231

Anderson BT (2007) On the joint role of subtropical atmospheric variability and equatorial subsurface heat content anomalies in initiating the onset of ENSO events. J Clim 20(8):1593–1599

Barnett T, Dümenil L, Schlese U, Roeckner E, Latif M (1989) The effect of Eurasian snow cover on regional and global climate variations. J Atmos Sci 46(5):661–686

Bellenger H, Guilyardi É, Leloup J, Lengaigne M, Vialard J (2014) ENSO representation in climate models: from CMIP3 to CMIP5. Clim Dyn 42(7–8):1999–2018

Bjerknes J (1969) Atmospheric teleconnections from the equatorial Pacific. Mon Weather Rev 97:163–172

Chang EK, Fu YF (2002) Interdecadal variations in Northern Hemisphere winter storm track intensity. J Clim 15(6):642–658

Chang EK, Guo Y, Xia X (2012) CMIP5 multimodel ensemble projection of storm track change under global warming. J Geophys Res 117:D23118. doi:10.1029/2012JD018578

Chen W, Li T (2007) Modulation of northern hemisphere wintertime stationary planetary wave activity: East Asian climate relationships by the quasi-biennial oscillation. J Geophys Res 112:D20120. doi:10.1029/2007JD008611

Chen W, Zhou Q (2012) Modulation of the Arctic Oscillation and the East Asian winter climate relationships by the 11-year solar cycle. Adv Atmos Sci 29:217–226

Chen W, Yang S, Huang R (2005) Relationship between stationary planetary wave activity and the East Asian winter monsoon. J Geophys Res 110:D14110. doi:10.1029/2004JD005669

Chen S, Chen W, Wei K (2013a) Recent trends in winter temperature extremes in eastern China and their relationship with the Arctic Oscillation and ENSO. Adv Atmos Sci 30:1712–1724

Chen S, Chen W, Yu B, Graf HF (2013b) Modulation of the seasonal footprinting mechanism by the boreal spring Arctic Oscillation. Geophys Res Lett 40:6384–6389. doi:10.1002/2013GL058628

Chen S, Yu B, Chen W (2014) An analysis on the physical process of the influence of AO on ENSO. Clim Dyn 42(3–4):973–989

Chen S, Wu R, Chen W, Yu B (2015a) Influence of the November Arctic Oscillation on the subsequent tropical Pacific sea surface temperature. Int J Climatol. doi:10.1002/joc.4288

Chen S, Yu B, Chen W (2015b) An interdecadal change in the influence of the spring Arctic Oscillation on the subsequent ENSO around the early 1970s. Clim Dyn 44(3–4):1109–1126

Chen S, Wu R, Chen W, Yu B, Xi Cao (2016) Genesis of westerly wind bursts over the equatorial western Pacific during the onset of the strong 2015–2016 El Niño. Atmos Sci Lett. doi:10.1002/asl.669

Cheung HN, Zhou W, Mok HY, Wu MC (2012) Relationship between Ural-Siberian blocking and the East Asian winter monsoon in relation to the Arctic Oscillation and the El Niño-Southern Oscillation. J Clim 25:4242–4257

Chiang JCH, Vimont DJ (2004) Analogous Pacific and Atlantic meridional modes of tropical atmosphere–ocean variability. J Clim 17:4143–4158

Choi K-S, Wu C-C, Byun H-R (2012) Possible connection between summer tropical cyclone frequency and spring Arctic Oscillation over East Asia. Clim Dyn 38(11–12):2613–2629

Deser C, Phillips AS, Tomas RA, Okumura YM, Alexander MA, Capotondi A, Scott JD, Kwon Y-O, Ohba M (2012) ENSO and Pacific decadal variability in the Community Climate System Model version 4. J Clim 25:2622–2651

Ding R, Li J, Tseng Y, Sun C, Guo Y (2015) The Victoria mode in the North Pacific linking extratropical sea level pressure variations to ENSO. J Geophys Res Atmos 120:27–45

Duchon CE (1979) Lanczos filtering in one and two dimensions. J Appl Meteorol 18(8):1016–1022

Feng J, Chen W, Tam CY, Zhou W (2011) Different impacts of El Niño and El Niño Modoki on China rainfall in the decaying phases. Int J Climatol 31:2091–2101. doi:10.1002/joc.2217

Feng JX, Wu ZH, Zou XL (2014) Sea surface temperature anomalies off Baja California: a possible precursor of ENSO. J Atmos Sci 71:1529–1537

Gao MN, Yang J, Gong DY, Kim SJ (2013) Unstable relationship between spring Arctic Oscillation and East Asian summer monsoon. Int J Climatol 34:2522–2528

Gill AE (1980) Some simple solutions for heat-induced tropical circulation. Q J R Meteorol Soc 106(449):447–462

Gong DY, Ho CH (2003) Arctic oscillation signals in the East Asian summer monsoon. J Geophy Res 108:4066. doi:10.1029/2002JD002193

Gong DY, Wang SW, Zhu JH (2001) East Asian winter monsoon and Arctic oscillation. Geophys Res Lett 28(10):2073–2076

Gong DY, Zhu J, Wang S (2002) Significant relationship between spring AO and the summer rainfall along the Yangtze River. Chin Sci Bull 47(11):948–952

Gong DY, Yang J, Kim SJ, Gao YQ, Guo D, Zhou TJ, Hu M (2011) Spring Arctic Oscillation–East Asian summer monsoon connection through circulation changes over the western North Pacific. Clim Dyn 37(11–12):2199–2216

Gong HN, Wang L, Chen W, Wu R, Wei K, Cui X (2014) The climatology and interannual variability of the East Asian winter monsoon in CMIP5 models. J Clim 27:1659–1678

Hu M, Gong DY, Mao R (2013) Possible influence of February–April Arctic Oscillation on the ITCZ activity of western-central Pacific. J Trop Meteorol 29:55–65 **(in Chinese)**

Huang R, Zhang R, Yan B (2001) Dynamical effect of the zonal wind anomalies over the tropical western Pacific on ENSO cycles. Sci China Ser D Earth Sci 44(12):1089–1098

Huang R, Chen W, Yang B, Zhang R (2004) Recent advances in studies of the interaction between the East Asian winter and summer monsoons and ENSO cycle. Adv Atmos Sci 21(3):407–424

Huang JY, Tan BK, Suo LL, Hu YY (2007) Monthly changes in the influence of the Arctic oscillation on surface air temperature over China. Adv Atmos Sci 24(5):799–807

Jeong JH, Ho CH (2005) Changes in occurrence of cold surges over East Asia in association with Arctic Oscillation. Geophy Res Lett 32:L14704. doi:10.1029/2005GL023024

Jin F (2010) Eddy-induced instability for low-frequency variability. J Atmos Sci 67(6):1947–1964

Jin F, Pan L, Watanabe M (2006a) Dynamics of synoptic eddy and low-frequency flow interaction. Part I: a linear closure. J Atmos Sci 63(7):1677–1694

Jin F, Pan L, Watanabe M (2006b) Dynamics of synoptic eddy and low-frequency flow interaction. Part II: a theory for low-frequency modes. J Atmos Sci 63(7):1695–1708

Kalnay E, Kanamitsu M, Kistler R, Collins W, Deaven D, Gandin L, Iredell M, Saha S, White G, Woollen J (1996) The NCEP/NCAR 40-year reanalysis project. Bull Am Meteorol Soc 77(3):437–471

Kim HJ, Ahn JB (2012) Possible impact of the autumnal North Pacific SST and November AO on the East Asian winter temperature. J Geophys Res 117:D12104. doi:10.1029/2012JD017527

Lau NC (1988) Variability of the observed midlatitude storm tracks in relation to low-frequency changes in the circulation pattern. J Atmos Sci 45(19):2718–2743

Lau NC, Nath MJ (1996) The role of the "atmospheric bridge" in linking tropical Pacific ENSO events to extratropical SST anomalies. J Clim 9(9):2036–2057

Lee SS, Lee JY, Wang B, Ha KJ, Heo KY, Jin FF, Straus DM, Shukla J (2012) Interdecadal changes in the storm track activity over the North Pacific and North Atlantic. Clim Dyn 39(1–2):313–327

Limpasuvan V, Hartmann DL (1999) Eddies and the annular modes of climate variability. Geophys Res Lett 26(20):3133–3136

Limpasuvan V, Hartmann DL (2000) Wave-maintained annular modes of climate variability. J Clim 13(24):4414–4429

Lin CY, Yu JY, Hsu HH (2015) CMIP5 model simulations of the Pacific meridional mode and its connection to the two types of ENSO. Int J Climatol 35:2352–2358

Linkin ME, Nigam S (2008) The North Pacific Oscillation–west Pacific teleconnection pattern: mature-phase structure and winter impacts. J Clim 21:1979–1997

Lorenz DJ, Hartmann DL (2003) Eddy-zonal flow feedback in the Northern Hemisphere winter. J Clim 16(8):1212–1227

Matsuno T (1966) Quasi-geostrophic motions in the equatorial area. J Meteorol Soc Jpn 44(1):25–43

Nakamura T, Tachibana Y, Honda M, Yamane S (2006) Influence of the Northern Hemisphere annular mode on ENSO by modulating westerly wind bursts. Geophys Res Lett 33:L07709. doi:10.1029/2005GL025432

Nakamura T, Tachibana Y, Shimoda H (2007) Importance of cold and dry surges in substantiating the NAM and ENSO relationship. Geophys Res Lett 34:L22703. doi:10.1029/2007GL031220

Nakamura T, Hara M, Oshika M, Tachibana Y (2015) Impact of the winter North Atlantic Oscillation (NAO) on the Western Pacific (WP) pattern in the following winter through Arctic sea ice and ENSO. Part II: multi-model evaluation of the NAO–ENSO linkage. Clim Dyn 45:3547–3562

Oshika M, Tachibana Y, Nakamura T (2015) Impact of the winter North Atlantic Oscillation (NAO) on the Western Pacific (WP) pattern in the following winter through Arctic sea ice and ENSO: part I—observational evidence. Clim Dyn 45:1355–1366

Park TW, Ho CH, Yang S (2011) Relationship between the Arctic Oscillation and cold surges over East Asia. J Clim 24(1):68–83

Rogers JC (1981) The North Pacific Oscillation. J Climatol 1(1):39–57

Smith TM, Reynolds RW, Peterson TC, Lawrimore J (2008) Improvements to NOAA's historical merged land-ocean surface temperature analysis (1880–2006). J Clim 21(10):2283–2296

Taylor KE, Stouffer RJ, Meehl GA (2012) An overview of CMIP5 and the experiment design. Bull Am Meteorol Soc 93(4):485–498

Thompson DW, Wallace JM (1998) The Arctic Oscillation signature in the wintertime geopotential height and temperature fields. Geophys Res Lett 25(9):1297–1300

Thompson DW, Wallace JM (2000) Annular modes in the extratropical circulation. Part I: month-to-month variability. J Clim 13(5):1000–1016

Thompson DW, Lee S, Baldwin MP (2003) Atmospheric processes governing the northern hemisphere annular mode/North Atlantic oscillation. Geophys Monogr AM Geophysl Union 134:81–112

Vimont DJ, Battisti DS, Hirst AC (2001) Footprinting: a seasonal connection between the tropics and mid-latitudes. Geophys Res Lett 28:3923–3926

Vimont DJ, Wallace JM, Battisti DS (2003) The seasonal footprinting mechanism in the Pacific: implications for ENSO. J Clim 16:2668–2675

Wallace JM, Gutzler DS (1981) Teleconnections in the geopotential height field during the Northern Hemisphere winter. Mon Weather Rev 109(4):784–812

Wang CZ, Weisberg RH (2000) The 1997–98 El Niño evolution relative to previous El Niño events. J Clim 13(2):488–501

Wang B, Wu R, Fu X (2000) Pacific-East Asian teleconnection: How does ENSO affect East Asian climate? J Clim 13(9):1517–1536

Weisberg RH, Wang C (1997) A western Pacific oscillator paradigm for the El Niño-Southern Oscillation. Geophys Res Lett 24(7):779–782

Woo S-H, Kim B-M, Jeong J-H, Kim S-J, Lim G-H (2012) Decadal changes in surface air temperature variability and cold surge characteristics over northeast Asia and their relation with the Arctic Oscillation for the past three decades (1979–2011). J Geophys Res 117(D18):D18117. doi:10.1029/2011JD016929

Wu B, Wang J (2002) Winter Arctic oscillation, Siberian high and East Asian winter monsoon. Geophys Res Lett 29(19):1897. doi:10.1029/2002GL015373

Wu R, Hu Z-Z, Kirtman BP (2003) Evolution of ENSO-related rainfall anomalies in East Asia. J Clim 16(22):3742–3758

Wu R, Yang S, Liu S, Sun L, Lian Y, Gao Z (2010) Changes in the relationship between Northeast China summer temperature and ENSO. J Geophys Res 115:D21107. doi:10.1029/2010JD014422

Xue X, Chen W, Chen S, Zhou D (2015) Modulation of the connection between boreal winter ENSO and the South Asian high in the following summer by the stratospheric quasi-biennial oscillation. J Geophys Res Atmos 120:7393–7411. doi:10.1002/2015JD023260

Yeh S-W, Kang Y-J, Noh Y, Miller AJ (2011) The North Pacific climate transitions of the winters of 1976/77 and 1988/89. J Clim 24(4):1170–1183

Yu B, Zwiers F (2007) The impact of combined ENSO and PDO on the PNA climate: a 1,000-year climate modeling study. Clim Dyn 29(7–8):837–851

Zhang Y, Wallace JM, Battisti DS (1997) ENSO-like interdecadal variability: 1900–93. J Clim 10(5):1004–1020

Zhou Q, Chen W, Zhou W (2013) Solar cycle modulation of the ENSO impact on the winter climate of East Asia. J Geophys Res Atmos 118:5111–5119. doi:10.1002/jgrd.50453

Zhu X, Dong W, Guo Y (2013) Comparison of simulated winter and spring arctic oscillation variability by CMIP5 and CMIP3 coupled models. Adv Clim Change Res 9:165–172

Zuo JQ, Li WJ, Ren HL (2013) Representation of the Arctic Oscillation in the CMIP5 models. Adv Clim Change Res 4(4):242–249. doi:10.3724/SPJ.1248.2013.242